Probing Charge Transfer Dynamics in All-organic Solar Cell Blends

A thesis by

Siddhartha Sohoni

Under the guidance of

Dr. Jyotishman Dasgupta

Dept. of Chemical Sciences

Tata Institute of Fundamental Research, Mumbai

Towards partial completion of the BS-MS dual degree of the

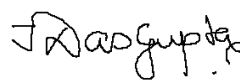## Indian Institute of Science Education and Research, Pune

CERTIFICATE

This is to certify that this dissertation entitled **Probing Charge Transfer Dynamics in All-organic Solar Cell Blends** towards the partial fulfilment of the BS-MS dual degree programme at the Indian Institute of Science Education and Research, Pune represents study/work carried out by Siddhartha Sohoni under the supervision of Dr. Jyotishman Dasgupta, Department of Chemical Sciences, Tata Institute of Fundamental Research, Mumbai during the academic year 2017-18.
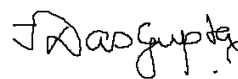
Siddhartha Sohoni

IISER Pune

Dr. Jyotishman Dasgupta

TIFR Mumbai

19th March 2018

DECLARATION

I hereby declare that the matter embodied in the report entitled **Probing Charge Transfer Dynamics in All-organic Solar Cell Blends** is the results of the work carried out by me at the Department of Chemical Sciences, Tata Institute of Fundamental Research, Mumbai under the supervision of Dr. Jyotishman Dasgupta and the same has not been submitted elsewhere for any other degree.

Siddhartha Sohoni

IISER Pune

Dr. Jyotishman Dasgupta

TIFR Mumbai

19th March 2018

INDEX

LIST OF FIGURES

Chapter 3

LIST OF TABLES

Chapter 3

ABSTRACT

Organic photovoltaics are a promising source of energy for the future generations. Commercially successful organic solar cells of today use fullerene derivatives as acceptors, or p-type materials. However, if the cost of solar derived electricity is to be brought down, and organic solar cell materials are to be used for this purpose, then we will have to move away from fullerenes and be able to fabricate polymer – polymer blend devices. In this project, we aim at replacing fullerene derivative acceptors from successful polymer – fullerene solar cell blends. The underlying mechanisms of charge transfer between donor and acceptor polymers are understood through transient absorption spectroscopy. When successful charge transfer is observed, all-polymer organic solar cell devices are fabricated and efficiency studies are carried out on them. Results indicate that more extensive optimisation of blend films is required in terms of thickness, morphology, solvent of film casting etc. in order to derive high efficiencies.

ACKNOWLEDGEMENTS

CHAPTER 1: INTRODUCTION

Fossil fuels, including natural gas, pose significant threats to the living conditions of future generations, and cannot be relied on in the long term for energy supplies due to their limited deposits on the planet. For these reasons, research in alternate fuels is of immense importance in today's age. Solar energy is one of the promising sources of renewable energy, and will be available to humankind till the existence of the sun. It is hoped that solar, wind and nuclear energy together can fulfil the entire energy needs of the planet in the near future.

The photovoltaic effect is responsible for the conversion of sunlight to voltage and charge carriers in a circuit. For this, a Type II junction is required in a material which absorbs in light in the region of the solar spectrum. Because of energy offsets between the n- and p- type materials' valence and conduction bands, charge separation takes place, with the photogenerated negatively charged carrier moving to the conduction band of the p- type and the positively charged carrier moving to the valence band in the n- type. These separated charges cannot recombine owing to the fact that they now exist in different materials. An external circuit can transport the negatively charged carrier from the conduction band of the p- type to the valence band of the n- type. This one way flow of current happens because of the energy difference between the p- type LUMO and the n- type HOMO (V_{OC}). Naturally, the voltage difference maintained across the external circuit is a function of this energy difference. A typical Type II junction is shown in figure 1.1.
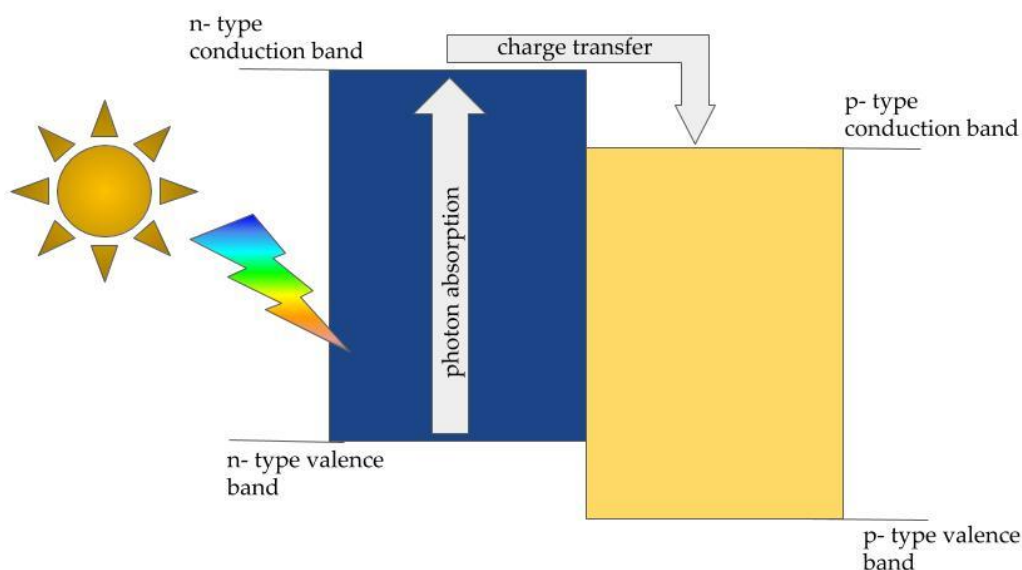
Figure 1.1: The photovoltaic principle. Photoexcitation of the n- type leads to charge transfer of the negatively charged carrier to the p- type conduction band. This is charge is obtained in the circuit.

The external quantum efficiency of the best performing perovskite solar cells that is achieved nowadays is close to 25%. Fundamental loss mechanisms within the materials set this upper limit on solar cell devices. These include heat dissipation through various channels like charge – phonon interactions.[1]

The most successful solar cell materials today are undoubtedly perovskites. Many reports claim efficiencies of perovskite devices which are close to the theoretical limit of the Carnot device. Commercially, crystalline silicon remains the frontrunner in spite of decades of research in the solar cell community. Crystalline silicon has a bandgap of 1.1 eV and absorbs in the 250 – 750 nm region of the solar spectrum. Robustness of silicon devices as opposed to perovskite devices makes silicon the favourite. However, silicon and other inorganic materials pose significant disadvantages resulting in solar derived energy being significantly more expensive than coal derived energy. For example, silicon is an indirect band gap material, has poor absorption cross sections through the entire range of the solar spectrum, and most importantly, is extremely difficult and expensive to fabricate in its crystalline,

defect-free form. Perovskites, on the other hand suffer from extreme sensitivity to moisture, and other environmental factors, and are far from environmentally benign because of the lead content in them.

In recent years, organic materials have been envisaged as possible ideal solar cell material candidates. The vast world of organic synthesis allows chemists a high degree of function specific tunability of properties. Moreover, organic materials are easier to synthesise in bulk as opposed to highly pure crystalline solids. They can be designed to be environmentally benign, and to absorb a significant chunk of all wavelengths in the solar spectrum. The field of organic photovoltaics aims at bringing down the cost of solar produced electricity drastically owing to the lowered environmental hazards, low cost of mass fabrication, and high tunability and efficiency of organic materials.[1, 2]

However, the mechanisms of generation of photocurrent and voltage in organic materials are different from those in the earlier described inorganic counterparts. Most inorganic materials are highly crystalline in nature. For this reason, the band structure in perovskites and silicon is well defined. As a result, the carrier in the conduction band is a well-defined entity in the wave vector space in the sense that a definite value of the magnitude of the k- vector can be easily assigned to this excited carrier. Its effective mass is also well known. The high degree of localisation in k- space leads to the carrier being highly delocalised in real space, and typical ranges of delocalisation of the conduction band carrier can be of the dimensions of the device in highly crystalline materials. In organic materials (especially polymers), such a long range order or crystallinity is difficult to achieve. Commonly, monocrystalline domains are of the order of a few hundred nanometers.[3] For this reason, neither does the carrier have a well-defined momentum, nor does it achieve the high levels of delocalisation on the crystal lattice.

Because of the low degrees of localisation, organic solar cell devices cannot be constructed by casting a layer of an n- type material on a p- type material followed by the placement of indium tin oxide. In such a situation, the photogenerated charge will not be able to reach the electrode. For the construction of organic solar cell devices, the n- type and p- type organic materials are dissolved together in an organic solvent, and directly spin coated on an indium tin oxide coated

surface. This forms nanodomains of intertwined p- type and n-type materials, and charge transfer can take place locally. This structure is known as the bulk heterojunction (BHJ). On photogeneration of a charge in an organic material blend, the negatively charged carrier and the positively charged carrier are localised within a radius of a few nanometers.[4] These spatially separated charges continue to strongly interact with each other. This happens because of a few reasons. First and foremost, because of the low crystallinity in organic blends, their band structure is highly heterogeneous and local minima in real space can trap these carriers. More often than not, the positive and negative charges end up in the same local minimum, creating the small radius of delocalisation.[5] For most organic materials, the dielectric constant is not as high as those found typically in ordered inorganic solids. This results in poor screening of Coloumbic interaction between the oppositely charged species. Due to this localisation, the charges interact intimately with each other and behave together as a quasiparticle.[6] This is called an exciton. Excitons obey Bose statistics because they are overall spin 1 particles.[7] Driven by several thermodynamic reasons as well as diffusion, the exciton generated within a nanodomain reaches the interface of the two materials. Because of the photovoltaic effect, the negatively charged carrier moves from the n- type to the p- type. This results in the dissociation of the exciton.[8] On dissociation, the typical distance between the negatively and positively charged carriers increases. However, the charges are known to reside at the interface for a duration of time because the Coulombic forces between them have still not been overcome.[4] In this timescale, the lattices of the two materials rearrange themselves to attain the lowest energy configuration while incorporating this charge within them. This lattice stabilised pair of charges within the two blends in known as a polaron pair, and when finally the Coulomb barrier is overcome, the separate charges in the materials are called polarons. The polarons then travel to the electrode and generate current. Needless to say, polarons, like electrons are fermions. Figure 1.2 depicts representations of an exciton and a polaron.
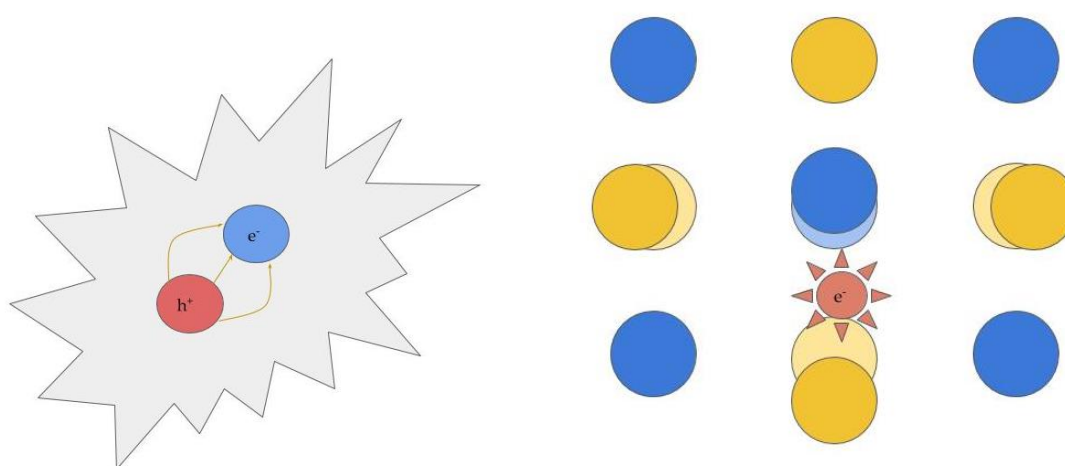
Figure 1.2: The first image shows a schematic of an exciton where h+ denotes the positively charged photogenerated carrier and e- denotes the negatively charged carrier. The second image shows a schematic of a polaron, where the blue and yellow lattice atoms have shifted in order to incorporate the negatively charged carrier and attain lowest energy configuration. This is a form of coupling between the phononic and carrier baths.

Certain additional loss pathways are inherent to organic solar cells due to the mechanism described earlier. The immediate recombination of the locally formed carriers within the blends is especially notorious. This is termed as geminate recombination, and is heightened is organic blends due to the localised trapping of the complementary charges. Another important loss mechanism is that of non-geminate recombination, which occurs when oppositely charged polarons meet and annihilate each other while diffusing to the electrodes. This loss can be attributed to the fact that blends contain randomly packed domains of p- and n- type materials.[1] For commercially successful organic solar cells to be fabricated, pathways to circumvent these loss mechanisms will have to be researched.

The photogeneration and subsequent charge transfer followed by charge collection at the electrodes are intimately connected to the excited state dynamics of these systems. Charge photogeneration is a Franck-Condon process. The localisation that follows this charge generation is ultrafast, and takes place on the

timescales of hundreds of femtoseconds typically in blends. Exciton diffusion also has timescales in picosecond regimes, and polaron generation takes place subsequently in nanosecond timescales.[8] In order to understand these mechanisms and dynamics in detail and to build sequential models, the excited state spectra of these materials need to obtained with sub-picosecond resolution. This is done through the technique of ultrafast broadband transient absorption spectroscopy.[2, 9] The technique is described in detail in the Methods and Materials chapter.

Most commonly used acceptor materials in organic photovoltaics are fullerene derivatives. [6, 6] –phenyl-C_{61} butyric acid methyl ester (PC$_{61}$BM), a successful fullerene based acceptor is shown in Figure 1.3. They owe their success to their low lying valence and conduction bands. They also form robust charge transport channels through extended coupling between aligned chromophores. Several successful organic solar cell blends have been reported wherein the fullerene derivatives have been used as acceptors.[4, 10]

However, fullerene derivatives pose significant disadvantages which cannot be overlooked if the earlier mentioned loss pathways have to be overcome, and a commercially successful organic solar cell is to be made. Fullerene derivatives have a negligible absorption cross section over the wavelength range of solar radiation. This means that they cannot participate in the photogeneration of charge carriers through hole transport. Synthesis procedures of fullerenes and their derivatives remain cumbersome, and are not entirely green and organic. Moreover, their small size makes them highly mobile within the blend and this affects the device efficiency over time, leading to robustness which is not comparable to silicon devices.[11]
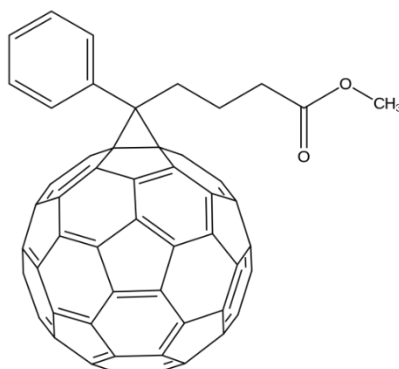
Figure 1.3: [6,6] -phenyl-C $_{61}$ butyric acid methyl ester (PC$_{61}$BM), a commercially successful fullerene derivative acceptor

In this project, we have attempted to replace fullerenes from commercially successful polymer – fullerene organic solar cell blends with a new polymer synthesised for the purpose of emulating acceptor properties and at the same time, circumventing challenges faced by fullerene acceptors, and to understand the subsequent charge transfer dynamics using transient absorption spectroscopy. We have also investigated partially the role of additives on all – polymer organic solar cell blends, and the effect of morphology on charge transfer through preliminary atomic force microscopy images.

We have investigated the possibilities of coupling our newly designed polymer with commercially successful donor materials, Poly(3-hexylthiophene-2,5-diyl) (P3HT) and Poly[[4,8-bis[(2-ethylhexyl)oxy]benzo[1,2-b:4,5-b']dithiophene-2,6-diyl][3-fluoro-2-[(2-ethylhexyl)carbonyl]thieno[3,4-b]thiophenediyl]] (PTB7) to form a successful all organic solar cell blend. Our polymer, 2DPP-OD-TEG (TEG) was synthesised by Prof. Satish Patil and group. Figure 1.4 (bottom) shows the molecular structure of TEG. The polymer features bandgaps comparable to those of fullerene derivatives, making it an ideal acceptor material. It shows activated transport up to very high temperatures, meaning that the conductivity of the polymer increases with increasing temperatures. The polymer also has a balanced ambipolar mobility making it a suitable candidate for efficient transport of polarons and excitons. The reported bandgaps obtained from ultraviolet photoelectron spectroscopy and cyclic voltammetry are -3.66 eV and -5.38 eV[12, 13]. In the project, P3HT and PTB7 are blended with TEG and excited state dynamics is observed using transient absorption spectroscopy. Devices are also made from P3HT – TEG blends to conduct current – voltage studies. TEG involves the linking of small molecule acceptors and donors in order to enhance transport. Finally, a PTB7 – TEG or P3HT – TEG blend has higher photon absorption in the solar radiation spectrum, meaning that a many more solar photons could be in principle converted to electrons in the circuit. Chemical structures of PTB7 and P3HT are depicted in Figure 1.4 (top). The bandgap alignments of PTB7, P3HT, PCBM and TEG are depicted in Figure 1.5. Figure 1.6 shows the advantage of TEG with respect to PCBM in terms of absorption in the range of solar radiation.
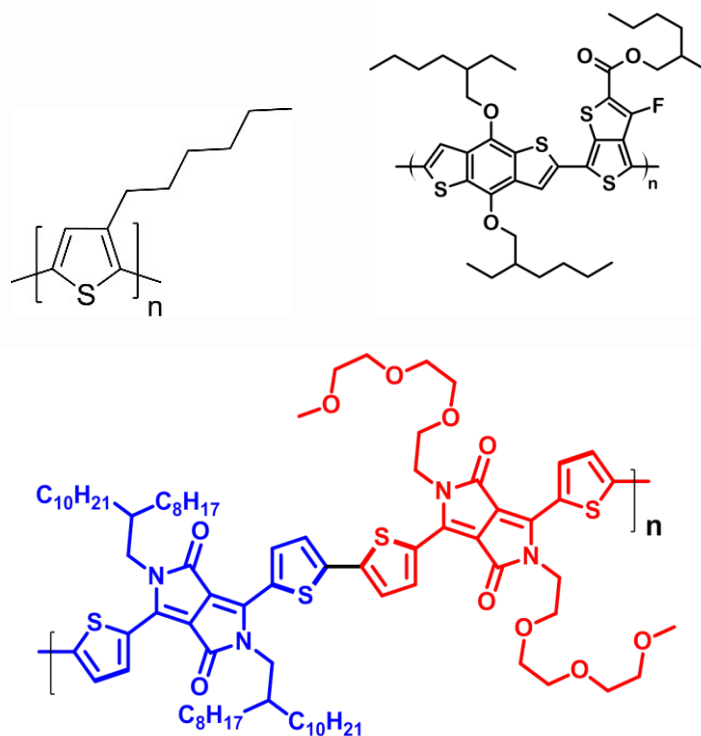
Figure 1.4: P3HT (top left), PTB7 (top right) and TEG (bottom). A small molecule donor (blue) and acceptor (red) are linked to in order to enhance thermodynamically driven transport.
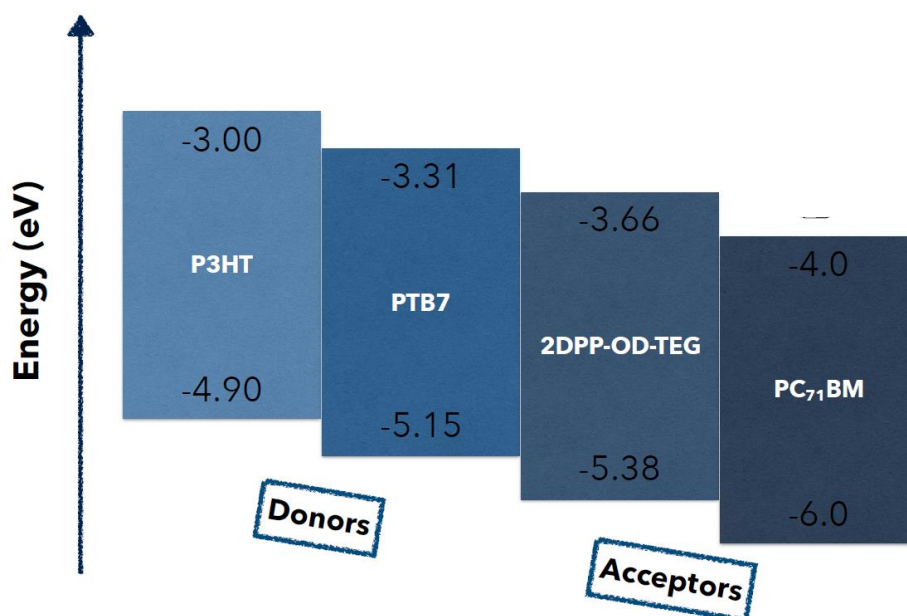
Figure 1.5: Band gaps of various materials used in this project.
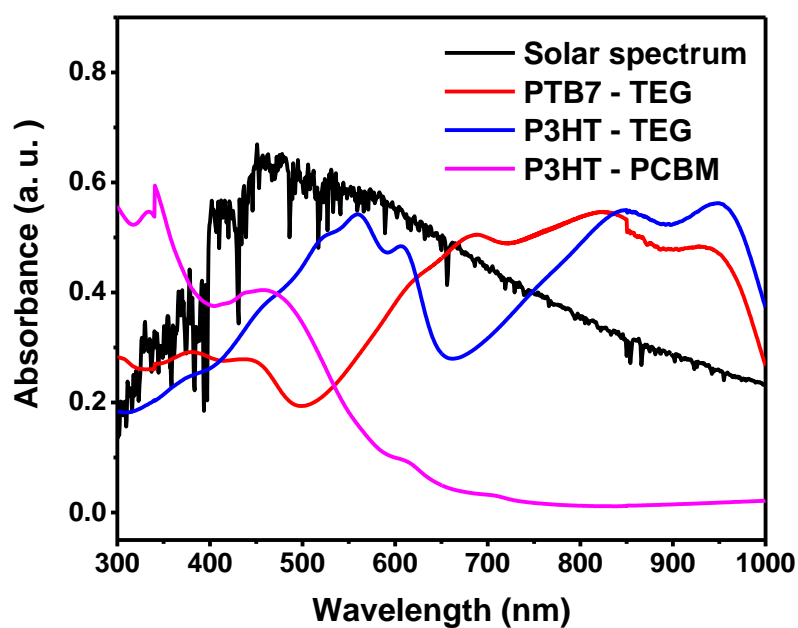
Figure 1.6: The black line indicates the solar spectrum. The red, blue and pink lines indicate absorption spectra of 1:2 weight by weight films of PTB7 – TEG, P3HT – TEG and P3HT – PCBM respectively. It is clear that non – fullerene materials are better suited for absorbing solar radiation.

CHAPTER 2: METHODS AND MATERIALS

As discussed in the earlier chapter, charge transfer in organic bulk heterojunction blends takes place in the excited states, or conduction bands of the donor and acceptor polymers. This is analogous to excited state reactions and to charge generation in perovskite solar cells.

To probe the fast dynamics of charges in excited states, we use the technique of sub-picosecond broadband transient absorption spectroscopy (TA). Using this technique, excited state dynamics can be directly observed with sub-picosecond time resolution. The technique was made possible with the advent of femtosecond laser pulses. In TA, the sample is first excited by a sub-picosecond laser pulse which corresponds to a wavelength in the region of the ground state absorption of the system. This pulse is transform limited and has a bandwidth in wavelength domain corresponding to the bandwidth in time domain, in accordance with the Fourier transform and Heisenberg relation for time and energy. The pulse excites a fraction of the population in the sample and higher electronic states, like S_1 or the conduction band are populated. To probe the excited state dynamics with temporal resolution, another sub-picosecond broadband pulse is impinged upon the sample with a variable time delay following the first pulse. We shall refer to the first pulse as the "pump" pulse and the second pulse as the "probe" pulse. The probe pulse is responsible primarily for two actions on the excited state population. Firstly, the weak probe pulse can excite the pump-excited molecules to higher electronic states, like S_2 for an example. This is called excited state absorption (ESA). Secondly, the probe pulse can also stimulate the emission of photons by stimulating the decay of the excited state population to the ground state. This is called stimulated emission (SE). These are illustrated in Figure. 2.1. The time delay between the pump and probe can be varied by changing the path difference between the pump and the probe and a 1.5 micron increase in path length corresponds to an increase in delay by 5 fs in air. The spectral detection is discussed in detail in the following paragraphs.[9]
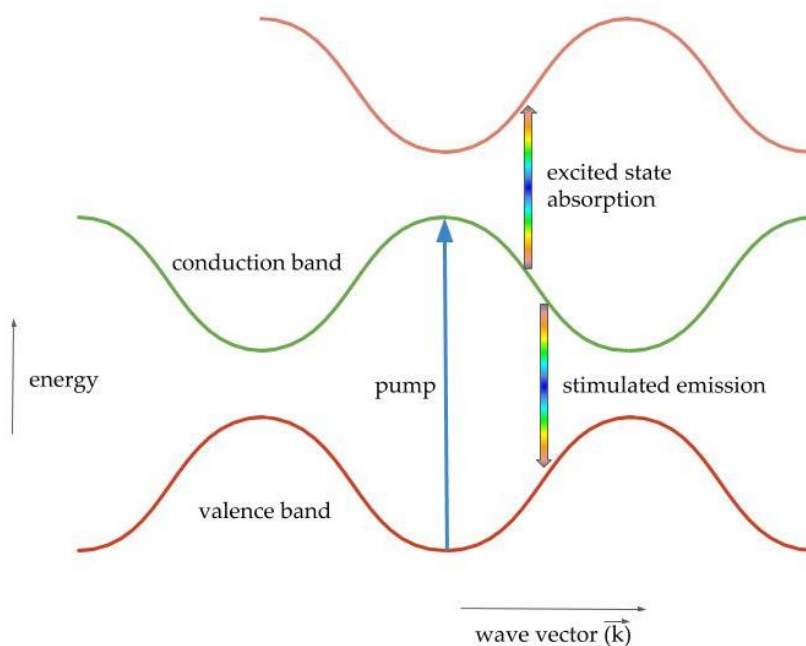
Figure 2.1: Excited state absorption (ESA) and stimulated emission (SE) due to the interaction of the sub-picosecond pump and the broadband sub-picosecond probe.

For a particular time delay, transient spectra are recorded in the following manner: First, the pump hits the sample and the probe hits following the time delay. The detector is phase matched with the probe in order to detect the probe photons. In the wavelength region where ESA takes place, probe photons decrease as some are absorbed by the excited state population. In the wavelength region where stimulated emission takes place, the probe photon count increases due to added photons which are emitted by the relaxing population (pump-on process). Following this, the pump is blocked and the probe is passed through the sample to the detector and the probe photon count is measured for all wavelengths in the absence of the pump pulse (pump-off process). Lastly, the pump-off probe spectrum is subtracted from the pump-on probe spectrum. This removes the envelope of the probe and direct spectra are obtained. However, in this process, one more factor comes into picture. When the pump is on, a fraction of the molecules is in the excited state. This means that the ground state absorption of the sample decreases in the presence of the pump pulse, as the excited state molecules do not participate in the ground state absorption. However, when the pump is off, the entire population participates in ground state absorption, leading to a higher ground state absorption in the absence of the pump. On subtracting the pump-off from the pump-on, a negative photon

count is obtained. This is called the ground state bleach. The ground state bleach (GSB) also reveals photo-induced dynamics of the system with the ground state population recovery. The negative of the pump-on – pump-off is plotted to obtain the change in absorbance of the sample at all wavelengths and is plotted as ΔA. Naturally, the GSB and SE show as negative features on the dA spectrum, whereas the excited state absorption shows as a positive feature. After this process, the time delay is increased and the process is repeated. In this manner, the kinetics of the various signatures is obtained. The process is illustrated in Figure 2.2 and Figure 2.3.
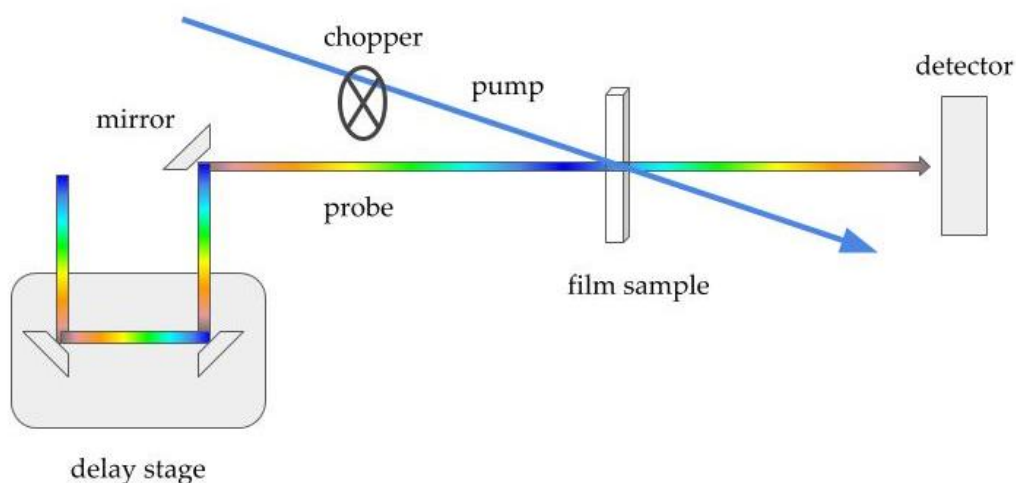
Figure 2.2: A schematic of the pump-probe setup used for broadband transient absorption spectroscopy. The chopper in the diagram is used to block alternate pump pulses in order to obtain the pump-off spectra, and the delay stage changes the time delay between pump and probe.

In Figure 2.3, the first inset shows a sample probe photon counts for the entire wavelength spectrum when the pump is blocked by the chopper. The second inset shows the probe counts of the same sample probe in the presence of the exciting pump pulse. The subtraction, pump-on – pump-off is shown in the last inset. This is the complete transient absorption spectrum for a given time point for the entire wavelength domain of the probe. The process is repeated for a different time delay and the spectrum is similarly recorded.
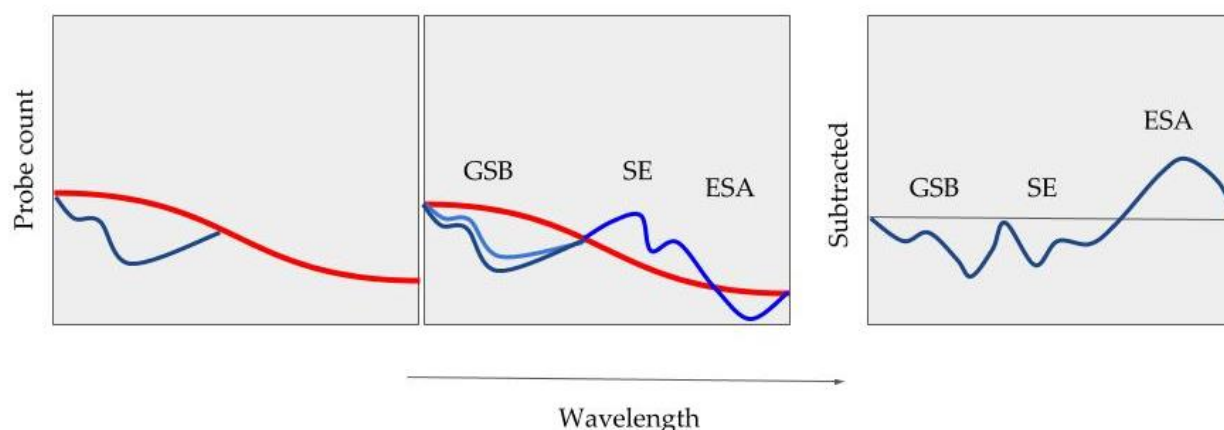
Figure 2.3: Sample probe photon counts on the wavelength domain of the probe for pump-on and pump-off measurements. The final inset shows their negative subtraction to plot the dA vs. the wavelength.

For this project, we have excited all materials around their ground state absorption maxima in order to obtain excited state dynamics of all donor and acceptor polymer films. These wavelengths are obtained from steady state absorption spectra plotted in Chapter 3. The pump power for all measurements has been kept between 0.005 and 0.02 mW after chopper. Low power measurements are made in order to obtain all spectra in the linear optical domain.[14]

Steady state absorption spectra are collected in the 300 – 1000 nm range using a spectrometer. The visible slit width for all measurements is 0.5 nm and the NIR slit width is 2 nm. For all measurements, absorbance is kept below 1 to ensure that all materials are probed in the linear Beer-Lambert behaviour.

The samples for transient absorption measurements are prepared following a uniform procedure. 20 mg/mL solutions are made of all polymers in chlorobenzene and are dropped slowly on quartz plates placed on the spin coater. The spin casting is done by the following procedure – one minute at 800 rpm with 400 rpm/s acceleration followed by two minutes at 2000 rpm with 800 rpm/s acceleration. The procedure is known to cast uniform thickness films with film thickness between 100 and 300 nm depending on the viscosity of the initial solution. Preliminary profilometry suggests film thickness of ~300 nm. However, more extensive atomic force microscopy measurements are required for accurate film thickness measurements.

Finally, to test the efficiency of our organic polymer blends in photovoltaic devices, we construct miniature solar cells in the following manner: Quartz plates (substrates) of uniform thickness are rinsed in freshly made piranha solution. The subsrates are then coated with a layer of indium tin oxide (ITO). After this, they are subjected to twenty minutes of ozone treatment in order to oxidise all impurities sticking to the quartz substrates. A layer of Zinc oxide is coated on top of the indium tin oxide using the pre-standardised zinc precursor (Zn(OTf)$_2$) solution. After deposition of zinc oxide, the films are annealed at 200 ^{o}C for 15 minutes. The device is then coated with the active layer of the polymer blend. This is done by spin coating at 100 rpm for 1 min with acceleration of 500 rpm/s. After this, the films are taken into an argon atmosphere glove box and annealed for 15 minutes at 140 ^{o}C. Then, they are placed in the thermal evaporator for deposition of silver from a silver pellet which is heated to a very high temperature in vacuum. This causes a fine layer of silver to deposit on the active layer. Finally, a layer of molybdenum oxide (MoO$_3$) is coated on the device. The thermal evaporator is preset to deposit a 100 nm layer of silver and 10 nm layer of molybdenum oxide. The device is then taken out of the argon glove box and IV measurements are carried out in a solar simulator. A schematic of the device is shown in Figure 2.4.
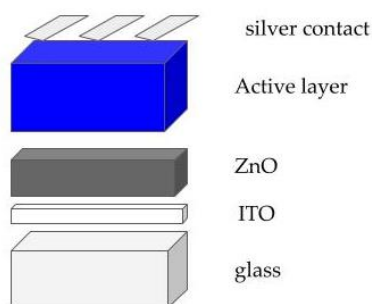
Figure 2.4: Architecture for devices. The active layer constitutes the polymer blends.

For kinetic fitting of signal, a multi-exponential decay function is used after convolution with an instrument response function. The instrument response function is takes into account the least count of time delay, the bandwidth of the pump and probe pulses, and any chirp that is caused due to the presence of wavelengths in excess of the transform limited bandwidth. The instrument response function has been measured earlier for our system, and for the purpose of fitting, is set as 0.1 ps.

Global analysis is a technique capable of manipulating the entire three dimensional surface obtained from transient absorption spectroscopy. The technique looks at the entire wavelength spectrum of the probe at all time points simultaneously, and matches similar decays for all wavelengths to construct spectra in the entire wavelength spectrum following the same decay. Hence, from the final spectra, the technique allows us to deconvolute two or three signals over the wavelength range that follow characteristically different kinetics, that can then be assigned to different species. In our case, a three component deconvolution is carried out to be able to isolate GSB, exciton and polaron signatures.[15]

PTB7, Zinc triflate, Indium tin oxide, chlorobenzene were purchased from Sigma Aldrich and used without further purification. TEG and squaraine derivatives are synthesized by Prof. Satish Patil's group at IISc, Bengaluru. We are thankful to Prof. Anil Kumar and group for providing us with highly crystalline pure P3HT which was used in this project.

Preliminary atomic force microscopy (AFM) is carried out in the tapping mode and more extensive AFM studies are required to understand morphology of the blends and its role in dictating device efficiency.

Device studies were carried out in Prof. Satish Patil's laboratory at the Solid state and Structural Chemistry at IISc, Bengaluru under the guidance of Aiswarya Abhisek Mohapatra. AFM studies are carried out in the Centre for Nanoscience and Engineering at IISc, Bengaluru. Global analysis on data has been carried out under the guidance of Dr. Palas Roy.

CHAPTER 3: RESULTS AND DISCUSSION

In order to temporally track charge transfer and separation between the donor PTB7 and the acceptor TEG, we carried out transient absorption measurements on pure PTB7, pure TEG and blend films of PTB7 and TEG. The blend films are made in 1:0.5, 1:1 and 1:2 weight ratios of PTB7 and TEG. In the rest of the thesis, they are referred to as described in Table 3.1. In order to decide the pump wavelength for the transient absorption measurements, steady state absorption spectra should be acquired first. To probe the transfer of the negatively charged carrier, the donor or n-type polymer should be excited at its absorption maximum, so as to create a significant population in the conduction band of the n- type. From this, charge transfer can take place to the p- type conduction band. These processes can be probed by looking at bleach recovery kinetics, excited state absorption kinetics for the exciton formed in the n- type conduction band, and the rise of the polaron signature in the transient spectra. To probe hole transfer from the p- type valence band to the n- type valence band, the acceptor p- type should be pumped at its wavelength of maximum absorption. This creates a population of holes in the p- type valence band, which can potentially transfer to stabilise uphill in the n- type valence band. Once again, the charge transfer process can be tracked by following the ground state bleach recovery kinetics, the exciton kinetics, and the polaron kinetics and rise time. Figure 3.1 shows steady state absorption spectra for pure PTB7, pure TEG and the PTB7 – TEG blends.

Legend:

Film name	PTB7 weight ratio	TEG weight ratio
PTB7	1	0
1:0.5	1	0.5
1:1	1	1
1:2	1	2
TEG	0	1

Table 3.1: Names of PTB7 – TEG films, and corresponding weight-by-weight ratios of the polymers in the films.

The pure PTB7 film shows absorption from 400 to 750 nm. In this, the absorption maximum in the 600 nm region corresponds to the valence band → conduction band transition with maximum Franck – Condon overlap wherein the wavenumber of the carrier changes precisely by $2\pi/a$, where 'a' is the box product of the lattice vectors. The absorption is of course dictated by the coupling term, $|<\psi_k|\hat{H}|\psi_{k\,+2\pi/a}>|^2$ where $\hat{H}$ is the perturbation Hamiltonian of the electromagnetic radiation, ψ_k is the carrier wavefunction for a carrier with wavenumber k in the valence band, and $\psi_{k\,+2\pi/a}$ is the wavefunction for the corresponding carrier at the same location in the Brillouin zone but in the conduction band. Note that this coupling term is in accordance with the Franck – Condon rule. The spatial part of the perturbation Hamiltonian is an odd function, and undoubtedly, in well-defined crystallinity, carriers of many wavenumbers will have non-zero coupling terms. This leads to vibrational resolution in the absorption spectra, and multiple peaks can be resolved, as is seen in the Figure 3.1. In solution also, PTB7 absorbs in a similar wavelength range. However, in the absence of crystallinity, multiple vibrationally resolved peaks are not seen. In solution in an isolated PTB7 molecule, the absorption at ~600 nm corresponds to the lowest energy $\pi \rightarrow \pi^*$ transition. In the pure TEG film, the absorption maxima in the 800 – 1000 nm region correspond to the valence band → conduction band ($\pi \rightarrow \pi^*$ in solution) transition, indeed convincing us that TEG is a low-bandgap polymer. The smaller absorption peak in the 300 – 400 nm region corresponds to transitions between inner electrons of the valence band and higher unfilled bands in the same

Brillouin zone. Herein, the wavenumber of the carrier changes by integral multiples of 2π/a. These transitions are not as symmetry allowed as the lowest energy transition, and in isolated molecules in solution, correspond to the σ → σ* transition. In the blends, no new charge transfer bands are seen, but this is not discouraging, as the photovoltaic effect requires charge transfer in the excited state. From the steady state absorption spectra, the pump wavelength used to track negative carrier transport will be the n- type absorption maximum, 620 nm, and the wavelength used to track hole transport will be the p- type absorption maximum, 810 nm. However, within organic photovoltaics, it is now known that the charge carrier experiences a bandlike potential in the ground and excited states in the early timescales. Following ultrafast localisation of the exciton within a sub-micron region, a localised, single molecule type potential is more applicable than a uniform crystal lattice for most organic materials.[2]
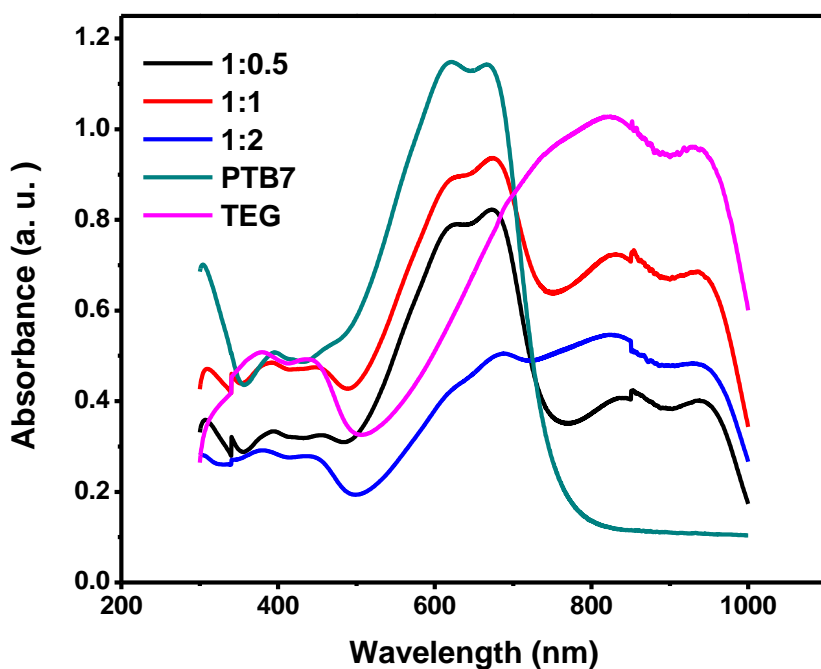

Figure 3.1: Steady state absorption spectra for PTB7:TEG blends.

Transient absorption spectra obtained on pumping the blend samples with 620 nm light are plotted in Figure 3.2. The probe range is from 800 to 1500 nm.
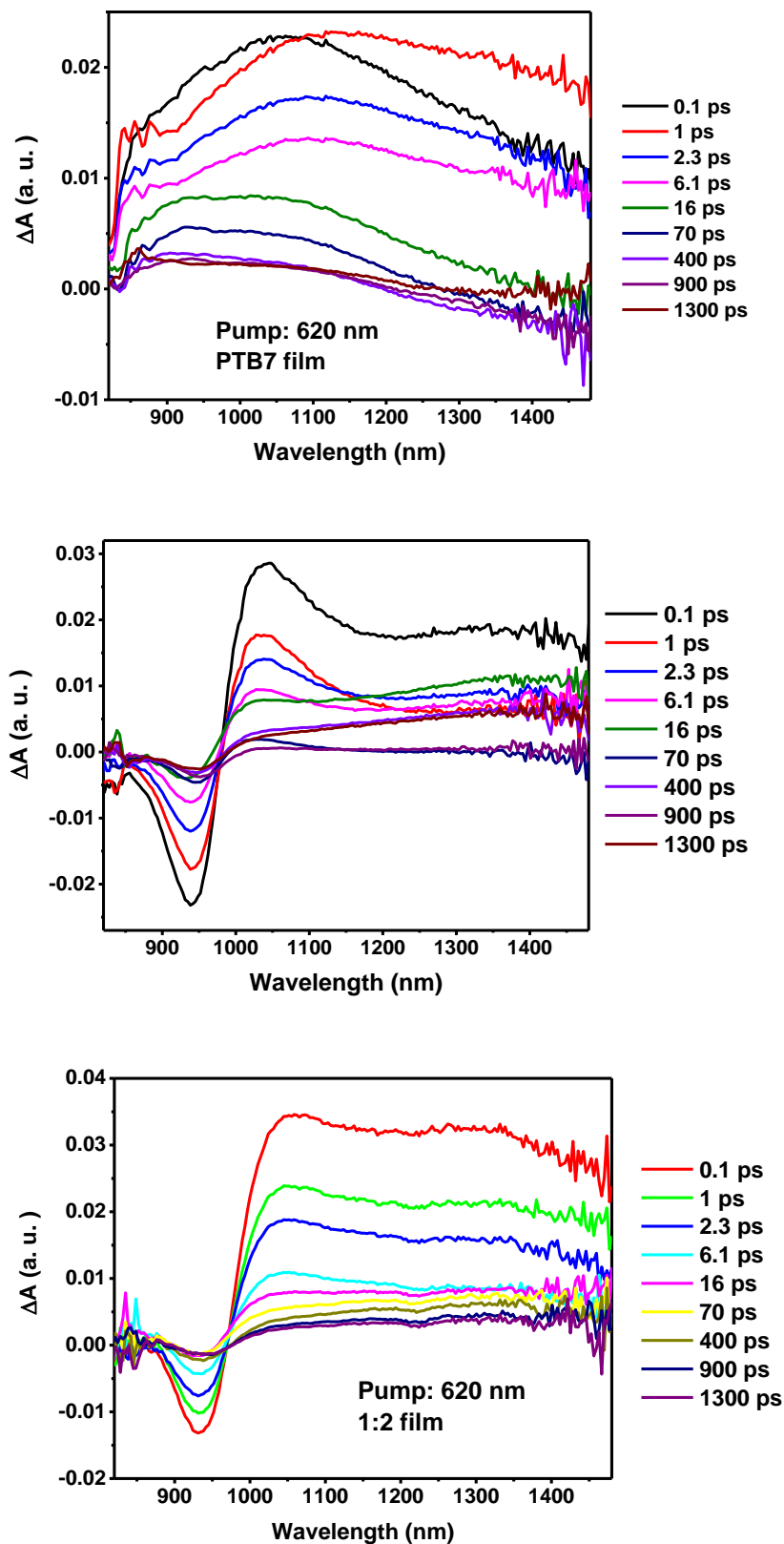
Figure 3.2: Transient spectra for various timepoints in the 800 – 1500 nm range on pumping PTB7, TEG and 1:2 blends at 620 nm.

The feature at ~1100 nm in the PTB7 film is identified at the PTB7 exciton. [16, 17] The feature at ~950 nm in the TEG film is identified as the ground state bleach of TEG. For the TEG film, the ~1350 nm feature is tentatively assigned as the TEG exciton and the ~1050 nm feature is assigned as the polaron. This assignment is carried out based on the fact that the 1350 nm signature decays faster than the 1050 nm signature. However, to be completely sure, detailed modelling will be required. The 1:2 spectra are a combination of these features along with any other features that arise due to interactions in the excited state. These spectra have also been recorded for the 1:0.5 and 1:1 films. The kinetics of signal decay are also plotted for various wavelengths, and shown in Figure 3.3.
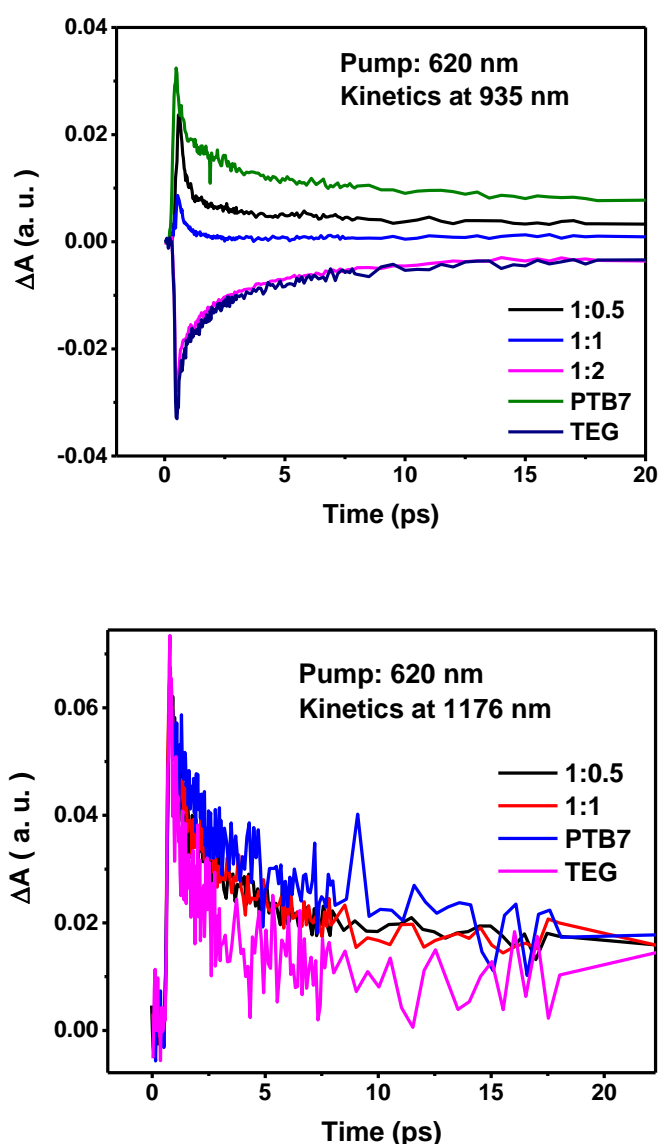
Figure 3.3: Signal decay kinetics at 935 nm (TEG ground state bleach) and 1176 nm (PTB7 exciton) in the early timescales.

As is evident from the decay of the PTB7 exciton signal, the addition of TEG acceptor does not drastically change the lifetimes. A two component fitting to these decays yields time components of 1.16 ps (48% weight) and 20 ps (37% weight) for the PTB7 film and 0.5 ps (53%) and 9 ps (32%) for the 1:2 film. The decay lifetimes for pure PTB7 and 1:2 match earlier reported data for decay of the exciton signal in PTB7. Transients are also obtained for the 810 nm pump. No negligible difference is seen in the ground state bleach recovery kinetics of the TEG on the addition of PTB7 in this data, which is not shown here. In any case, in the absence of negative charge carrier transfer from PTB7 to TEG, which is evident from the plotted data, it can be concluded that in the current film morphology, the visible photons in the PTB7 absorption range will not contribute to charges in the circuit.

Because substantial change is not observed in exciton decay kinetics in PTB7 on addition of the TEG acceptor, we move to another successful fullerene blend, that of P3HT with fullerenes, and proceed by replacing the fullerene with TEG. For this, we make P3HT – TEG films of various weight ratios, which are summarised in Table 3.2.

Film name	P3HT weight ratio	TEG weight ratio
P3HT	1	0
1:0.5	1	0.5
1:1	1	1
1:2	1	2
TEG	0	1

Table 3.2: Names of P3HT – TEG films, and corresponding weight-by-weight ratios of the polymers in the films.

As in the earlier case, we proceed with steady state absorption characterisation of the blend films. Absorption spectra for the different ratios of weight by weight P3HT – TEG blends are shown in Figure 3.4.
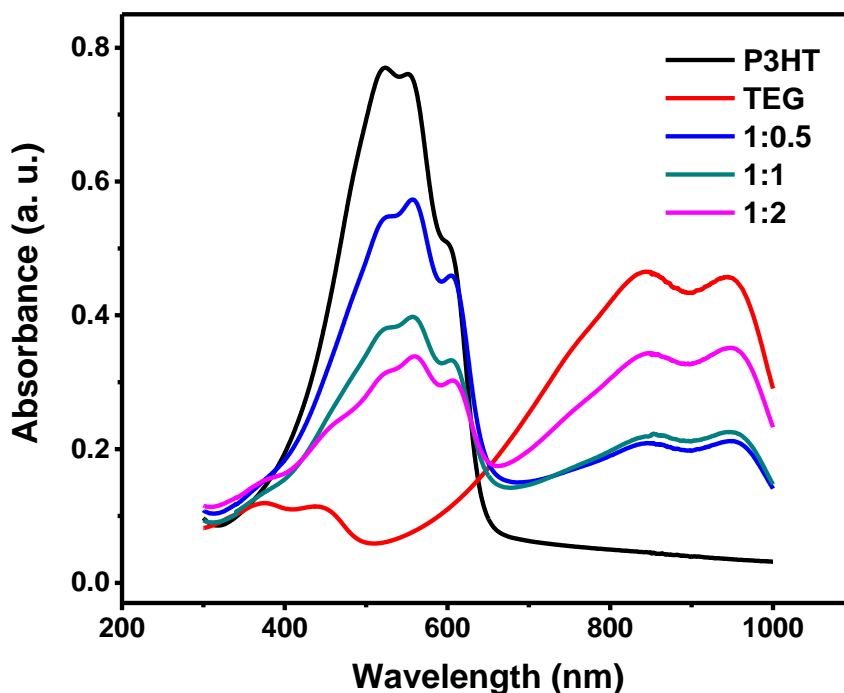
Figure 3.4: Steady state absorption spectra for P3HT – TEG blends.

In the pure P3HT film, the valence band → conduction band (π → π* in solution) transition is seen between 400 and 600 nm, with an absorption maximum at ~520 nm. As in the case of PTB7, the absorption spectrum is vibrationally resolved and shows three peaks. This resolution is an indicator that the film is crystalline in character. The pure TEG film absorption is also plotted again and is the same as the earlier obtained curve. The existence of an isosbestic point at ~620 nm for these films indicates that in the ground state, the absorption of the P3HT and TEG are not affected by the other's presence, and that ground state charge transfer is not taking place. From the steady state absorption data, the pump wavelengths are decided to be 520 nm and 820 nm for observing negative charge transfer and hole transfer between the blends respectively, as these are the absorption maxima of the donor and the acceptor. Figure 3.5 shows the transient data obtained on pumping the donor at 520 nm in the blends, and in neat films. Note that due to a non-zero absorption for TEG at 520 nm, a ground state bleach is observed for TEG even in case of donor pumping, which means that the 520 nm light inadvertently pumps a
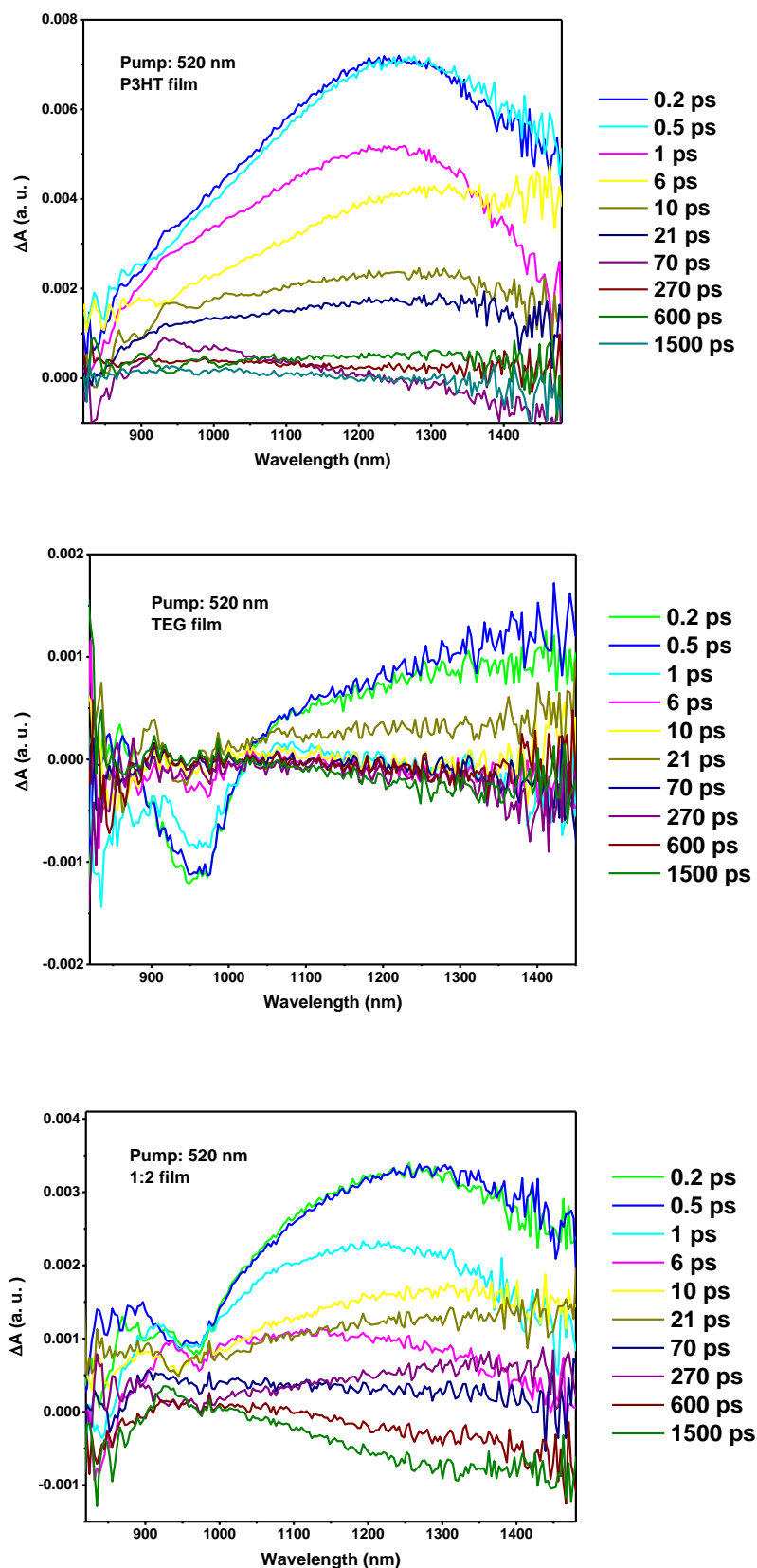
Figure 3.5: Transient spectra for various timepoints in the 800 – 1500 nm range on pumping P3HT, TEG and 1:2 blends at 520 nm.

small fraction of acceptor molecules to the excited state along with the donor molecules.

Again, the negative feature at ~950 nm in the TEG film is the ground state bleach. The positive feature at ~1250 nm in the P3HT film at early times is the P3HT exciton. At later time points, a new feature can be seen at ~950 nm, which is the P3HT polaron. The 1:2 spectra can contain all these peaks. On successful charge transfer between from P3HT to TEG, the P3HT polaron signature at 1000 nm should be enhanced in the blend film, as is seen in later time points in the blend.[10] Kinetics are plotted for the various blends at 945 nm on 520 nm pumping. If a large fraction of the P3HT exciton converts to polarons, then a change will be seen in the decay kinetics of the wavelengths of the polaron signature. Figure 3.6 shows the signal decay kinetics at 945 nm for the various blends.
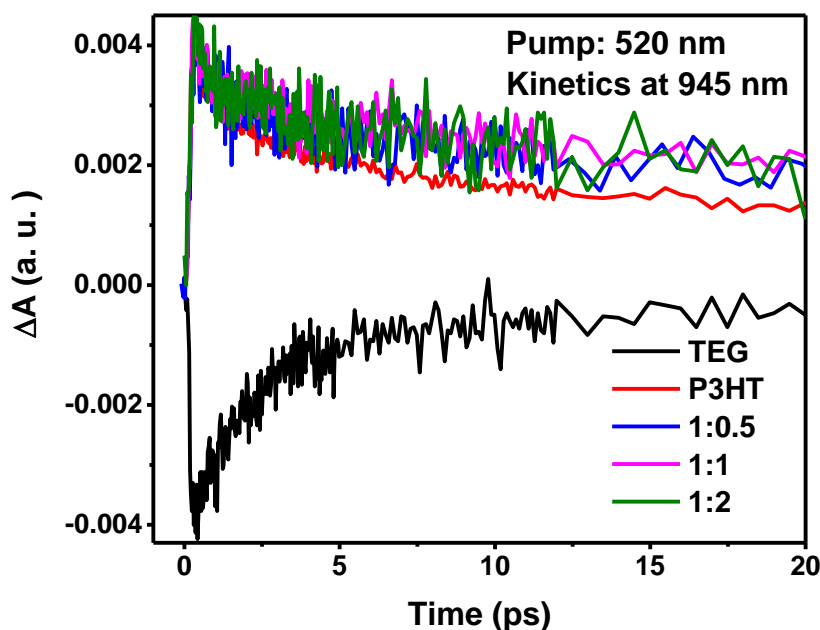
Figure 3.6: Kinetics of signal decay at 945 nm. The graph shows decay kinetics for the various blends

However, the ~950 nm P3HT polaron peak is convoluted with the ground state bleach of TEG, and curve fitting of decay kinetics will also factor the ground state bleach recovery of the TEG. In order to get around this, weighted TEG and

P3HT spectra for the same time points are subtracted from the 1:2 spectra for the same time point.[8] This procedure is only possible at early timepoints, as the low signal-to-noise ratio at later timepoints does not allow clean subtraction. Figure 3.6 shows the subtracted spectra.
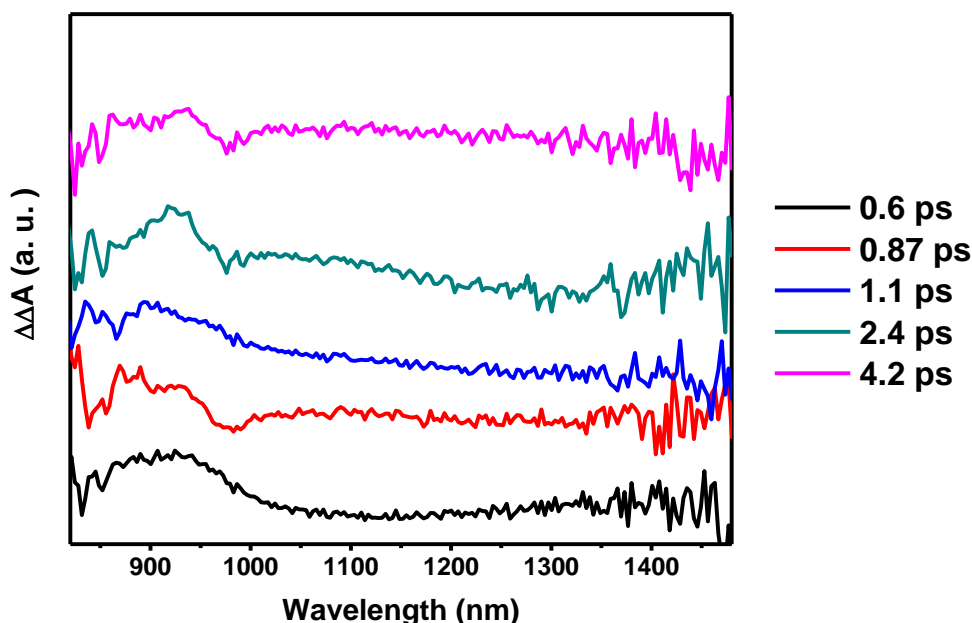
Figure 3.7: 1:2 blend transient spectra after subtraction of the pure P3HT and TEG components for the same timepoints.

A clear new feature can be seen between 900 and 1000 nm, and matches well with reported values of the P3HT polaron peak.[8, 10] This new peak also matches excellently with the steady state absorption spectra of $FeCl_3$ oxidised P3HT suggesting that they arise from the formation of holes within the P3HT molecule.[8] This result clearly indicates charge separation between the two polymers, as the polaron yield is significantly higher. To further deconvolute the ground state bleach and polaron signatures, global analysis is carried out on the transient absorption data for the 1:2 blend film. In a three component fitting, the polaron signal is also obtained. The global analysis generated signals can be seen in Figure 3.7. The advantage of carrying out global analysis is that the contribution of the polaron signal can also be isolated at the later timepoints.
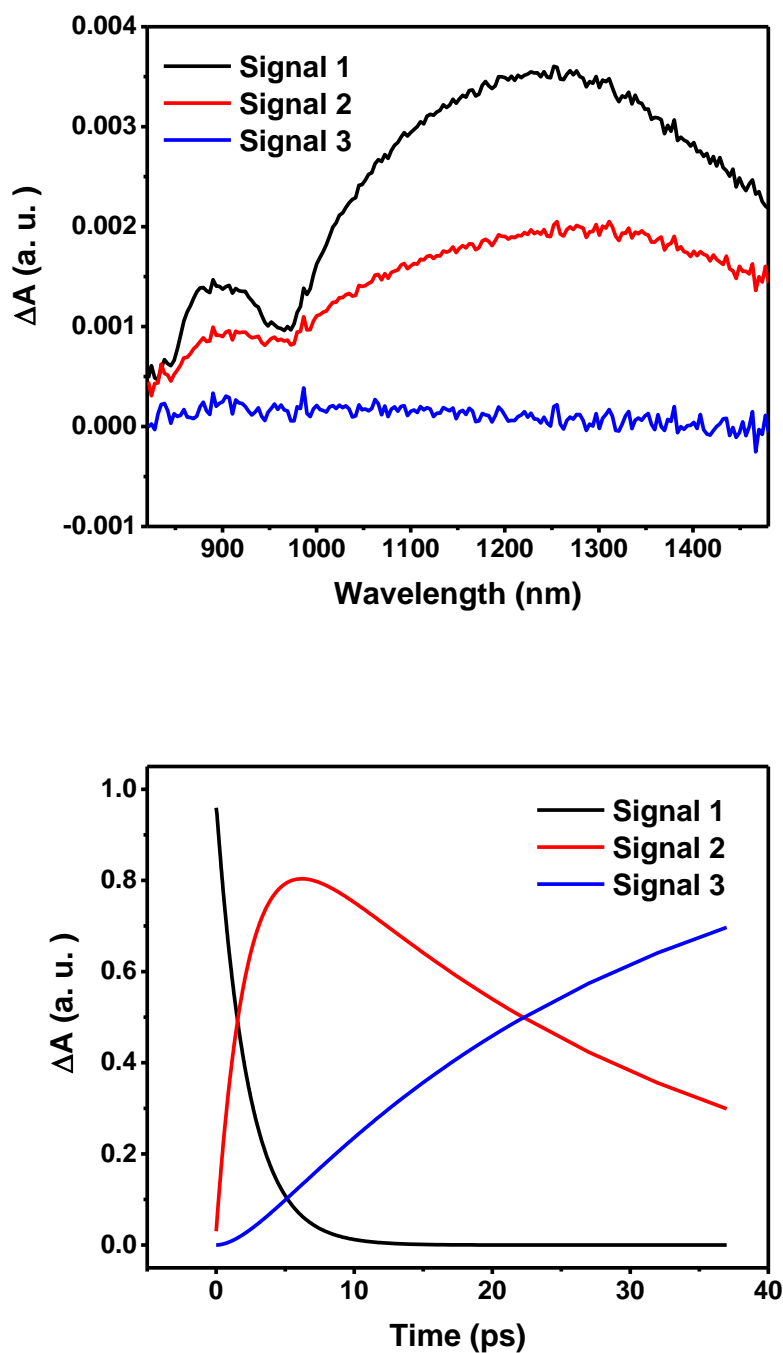
Figure 3.8: The first graph shows the three isolated signals obtained from global analysis of the transient data of the 1:2 film on 520 nm pumping. The second graph shows the kinetics of decay and evolution of the three signals. Signal 3 corresponds to the polaron.

Due to the high molar absorptivities of the other excited state features, the polaron signature gets masked in this analysis. The different kinetics of these signals are

shown in Figure 3.8, and Signal 3 corresponds to the polaron. As is expected, the polaron signature shows a rise time, attributed to the diffusion of the exciton to the interfaces. Note that the kinetics generated by the analysis are normalized.[3, 8]

Encouraged by this result, we fabricated devices for various P3HT – TEG blends with the same film casting protocol, as described in Chapter 2. For devices, a squaraine additive is also used in a low weight ratio.[18] The bandgaps of the squaraine molecule are aligned to be between those of P3HT and TEG.[19] Reports suggest that squaraines form J- aggregates in blends and aid the formation of well-defined donor and acceptor nanodomains to increase overall blend efficiency.[18, 20] The particular squaraine molecule used by us is shown in Figure 3.9. Figure 3.10 shows the J-V light and dark curves for the best performing P3HT – squaraine – TEG device of the P3HT:squaraine:TEG weight ratio of 1:0.1:2. Devices for various other P3HT – squaraine – TEG ratios are also fabricated. For J – V studies, the solar simulator is optimized for actual earth conditions using a known P3HT – PCBM device.
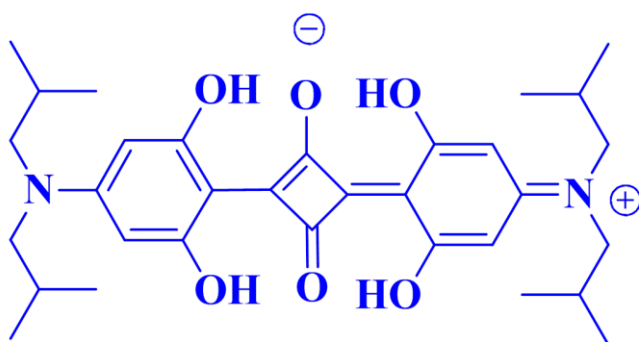

Figure 3.9: Squaraine derivative used as additive in devices to increase efficiency.
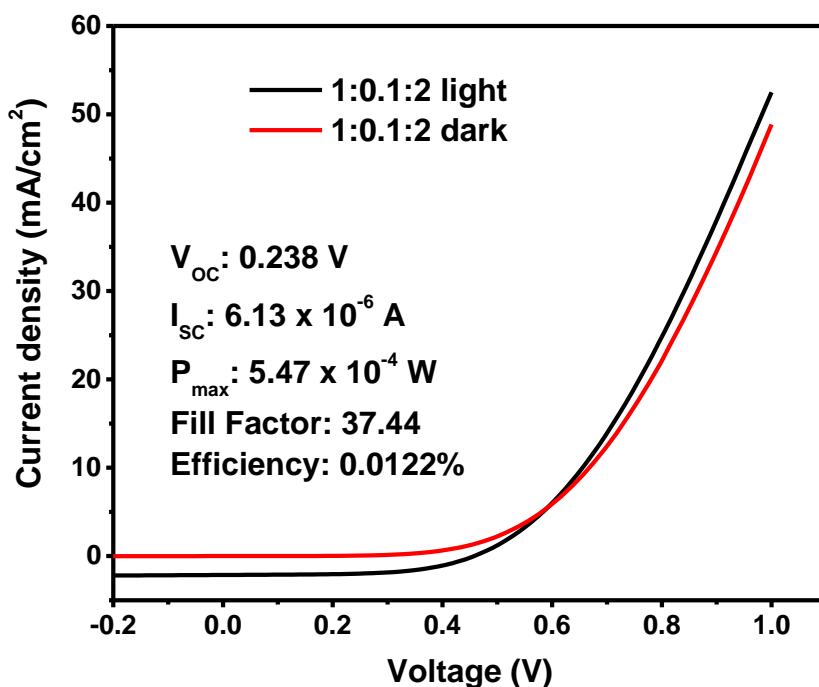
Figure 3.10: J-V data for a 1:0.1:2 P3HT:squaraine:TEG blend device.

For most solar cell devices, a very low efficiency of the range of 0.01% is obtained. The best efficiency obtained is 0.0122%. The fill factor is low at 37, and the open circuit voltage (V_{OC}) and short circuit current (I_{SC}) are also unremarkable, resulting in a low maximum power (P_{max}). However, it should be noted that these are preliminary studies and optimization for device efficiency is yet to be carried out. The encouraging information from the J-V data is that a Type II junction forms between the two polymers, and amplification also takes place, suggesting that the blend is not a pure resistor.

Following this, transient absorption studies are carried out with 820 nm pumping to observe any possible hole transfer between the valence bands of TEG and P3HT. The spectra of the TEG and 1:2 films for 820 nm are shown for various time points in Figure 3.11.
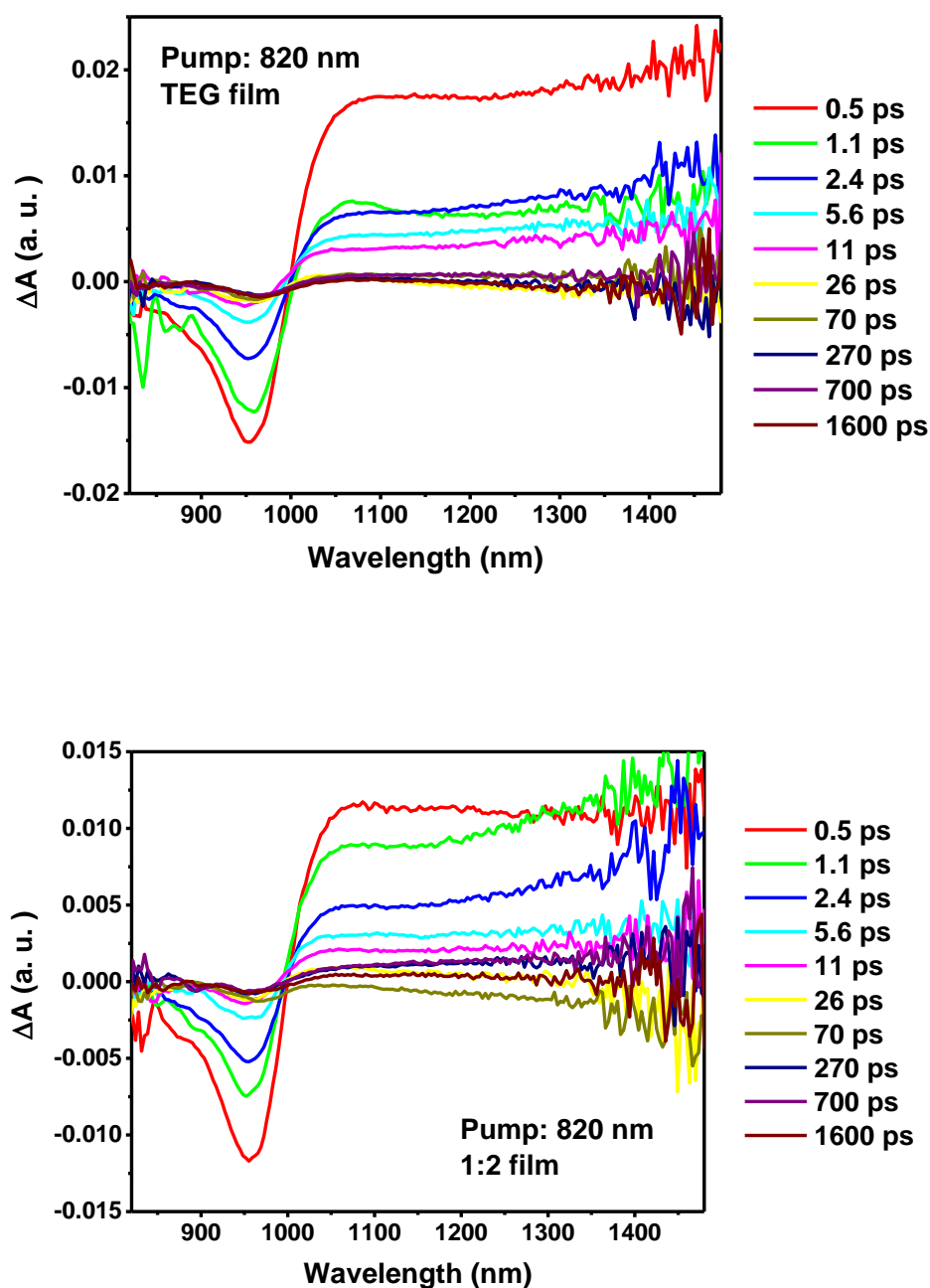
Figure 3.11: Transient spectra for various timepoints in the 800 – 1500 nm range on pumping TEG and 1:2 blends at 820 nm.

The negative feature in the ~950 nm region is attributed to the ground state bleach of TEG and the ~1100 nm feature is assigned as the TEG exciton. If a donor – acceptor system shows hole transfer from the acceptor valence band to the donor valence band, then this is most visibly captured in the kinetics of the ground state bleach

recovery of the acceptor species. In the presence of hole transfer to the donor, the ground state bleach of the acceptor will recover more slowly as compared to a pure acceptor's bleach. Kinetics are plotted for the ground state bleach of TEG at 952 nm and look almost identical for blends, suggesting that hole transfer is absent.
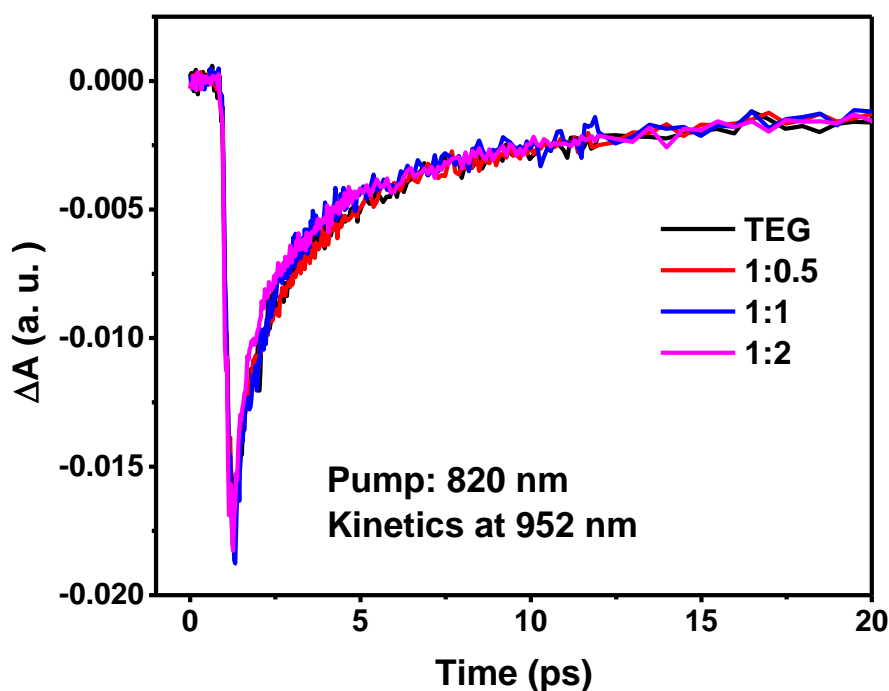
Figure 3.12: Signal decay kinetics at 952 nm (TEG ground state bleach) in the early timescales.

Kinetic fitting for all blends yields two time components of 0.6 ps (65% weightage) and 7 ps (35%). This suggests that the photons absorbed in the near infrared (NIR) region of the solar spectrum are not contributing to charges in the circuit, reducing the role of the acceptor polymer to that of the fullerene. While this is not the expected result, it should be noted that the blend films have not been optimised with respect to morphology in order to obtain hole transfer.

Lastly, to know the size of nanodomains in the P3HT – squaraine – TEG blends, preliminary tapping mode atomic force microscopy is carried out on the films. The AFM images are shown in Figure 3.13.
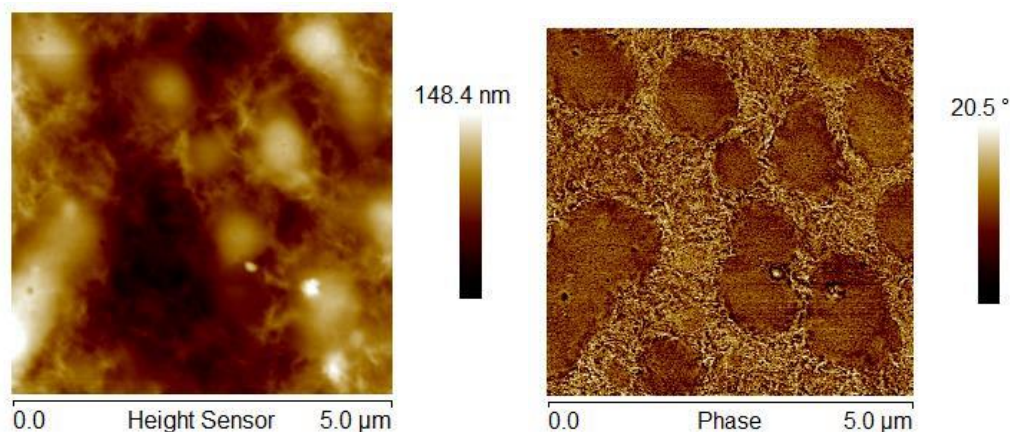
Figure 3.13: Atomic force microscopy images of 1:0.1:2 P3HT:squaraine:TEG films. The left image shows height, and the right image shows phase.

In tapping mode AFM, the AFM tip oscillates with a certain frequency and amplitude in space in order to record the topography of the substrate. The substrate adds a lag component to this frequency due to non – conservative interactions (friction, stickiness). Different materials change the phase of the tip oscillations to different extents. Therefore, tapping mode AFM can also give us this phase information, which correlates to different materials in the substrate, along with the substrate topography. As is seen in the AFM image of the P3HT – squaraine – TEG film optimised for devices, the nanodomains formed of the different materials are of the size order of a few microns. Recent work by Nilay Hazari, Andre Taylor and group shows a strong correlation of the size of nanodomains with the device efficiency. Herein, they show that on formation of smaller (~150 nm) sized nanodomains, with well separated donor and acceptor phases, the efficiency of blend devices increases.[18] In their work, larger, less phase separated domains show lower efficiency. We see that in our 1:0.1:2 P3HT – squaraine – TEG blend too, phase separation is not clear, and domain sizes are of the order of a few micrometers. In larger sized domains, as in our case, non – geminate recombination predominates, resulting in low V_{OC} and I_{SC} values. Extensive optimisation can be carried out for film casting procedures by looking at morphology through AFM for achieving sub-micrometer sized domains. This could lead to better hole and negative carrier separation in blends, and higher efficiencies in devices.

CHAPTER 4: CONCLUSIONS

In this project, we have started out with the idea of fabricating a third generation solar cell which is all organic. As is the defining characteristic of third generation solar cells, we have tried to maximize photon absorption through the entire spectral range of solar radiation incident on the earth.[1] We have adopted the strategy of looking at successful polymer – fullerene solar cell blends and replacing the fullerenes[21] with a new NIR absorbing acceptor polymer, 2DPP-OD-TEG. We have studied the subsequent excited state dynamics in blends of P3HT with 2DPP-OD-TEG and have achieved an encouraging result of negative charge carrier transfer between the two blends on optically exciting the P3HT donor. Following this, we have fabricated devices and carried out J-V studies on them. Our devices show efficiencies of the order of ~0.01%. Although this number is low at the moment, further optimization can be carried out to increase this. For example, it is suggested that solvents offering reduced and differential solubility of the materials during spin casting result in sharper and smaller nanodomains, which in turn increase efficiency. In our case, all films are cast using chlorobenzene as solvent. Other solvents can be investigated for better separation of the two polymer phases. Reasonable doubt can also be raised about the actual band energy value of the TEG polymer, as values obtained from cyclic voltammetry and UPS are known to be inconsistent with each other for organic polymers. Also as polymers most likely arrange in different crystal structures in blends and pure films, direct band gap measurements should be carried out on the blends.[1] In the case that P3HT – TEG do not form a Type II junction with an offset of 0.3 eV between them, which is generally required for organic polymers, then other donor polymers or small molecules can also be explored.[22] Lastly, the quantum efficiency of charge transfer between these polymers should be calculated, either using upconversion or transient Kerr-gated emission techniques.[23]

Finally, TEG possesses unique properties which include a high ambipolar mobility, high robustness, a high range of temperature for activated transport, and unique NIR absorption. For these numerous reasons, the use of TEG in organic solar cells should be further explored extensively.

REFERENCES

1. S. Matthew Menke, N. A. Ran, G. C. Bazan and R. H. Friend, *Joule,* 2017,**2,** 25 - 35

2. N. Banerji, *J. Mat. Chem. C,* 2013,**18,** 3045 – 3168

3. S. B. Penwell, L. D. S. Ginsberg, R. Noriega and N. S. Ginsberg, *Nat. Mater.,* 2017,**16,** 1136 – 1141

4. A. C. Jakowetz, M. L. Bohm, A. Sadhanala, S. Huettner, A. Rao and R. H. Friend, *Nat. Mater.,* 2017,**16,** 551 – 557

5. S. Gelinas, A. Rao, A. Kumar, S. L. Smith, A. W. Chin, J. Clark, T. S. van der Poll, G. C. Bazan, R. H. Friend, *Science,* 2014,**343,** 512 – 516

6. I. Constantinou, X. Yi, N. T. Shewmon, E. D. Klump, C. Peng, S. Garakyaraghi, C. K. Lo, J. R. Reynolds, F. N. Castellano and F. So, *Adv. Energy Mater,* 2017,**7,** 1601947 – 1601953

7. L. Ju, L. Wang, T. Cao, T. Taniguchi, K. Watanabe, S. G. Louie, F. Rana, J. Park, J. Hone, F. Wang and P. L. McEuen, *Science,* 2017,**358,** 907 – 910

8. P. Roy, A. Jha and J. Dasgupta, *Nanoscale,* 2016,**8,** 2768-2777

9. J. Cabanillas-Gonzalez, G. Grancini and G. Lanzani, *Adv. Mater.,* 2011,**23,** 5468 – 5485

10. S. M. Falke, C. A. Rozzi, D. Brida, M. Maiuri, M. Amato, E. Sommer, A. D. Sio, A. Rubio, G. Cerullo, E. Molinari and C. Lienau, *Science,* 2014,**344,** 1001 – 1005

11. A. F. Eftaiha, J. Sun, I. G. Hill and G. C. Welch, *J. Mater. Chem. A*, 2014,**2,** 1201-1213

12. S. P. Senanayak, A. Z. Ashar, C. Kanimozhi, S. Patil and K. S. Narayan, *Phys. Rev. B.,* 2015,**91,** 115302 – 115318

13. C. Kanimozhi, N. Yaacobi-Gorss, K. W. Chou, A. Amassian, T. D. Anthopoulos and S. Patil, *J. Am. Chem. Soc.,* 2012,**134,** 16532 – 16535

14. R. Berera, R. van Grondelle and J. T. M. Kennis, *Photosyn Res.,* 2009,**101,** 105 – 118

15. I. H. M. van Stokkum, D. S. Larsen and R. van Grondelle, *Biochim. Biophys Acta,* 2004,**1657,** 82 - 104

16. N. Zarrabi, P. L. Burn, P. Meredith and P. E. Shaw, *J. Phys. Chem. Lett.,* 2016,**7,** 2640 – 2646

17. J. M. Szarko, B. S. Rolczynski, S. J. Lou, T. Xu, J. Strzalka, T. J. Marks, L. Yu and L. X. Chen, *Adv. Funct. Mater,* 2014,**24,** 10 – 26

18. J. Huang, T. Goh, X. Li, M. Y. Sfeir, E. A. Bielinski, S. Tomasulo, M. L. Lee, N. Hazari and A. D. Taylor, *Nat. Photonics,* 2013,**7,** 479 – 485

19. G. Chen, H. Sasabe, Y. Sasaki, H. Katagiri, X. Wang, T. Sano, Z. Hong, Y. Yang and J. Kido, *Chem. Mater.,* 2014,**26,** 1356 – 1364

20. G. de Miguel, M. Ziolek, M. Zitnan, J. A. Organero, S. S. Pandey, S. Hayase and A. Douhal, *J. Phys. Chem. C.,* 2012,**116,** 9379 – 9389

21. T. J. Siso, Y. Zhong, B. Zhang, M. T. Trinh, K. Miyata, X. Zhong, X. Y. Zhu, M. L. Steigerwald, F. Ng and C. Nuckolls, *J. Am. Chem. Soc.,* 2017,**139,** 5648 – 5651

22. W. Li, K. H. Hendriks, A. Furlan, Martijn M. Wienk and R. A. J. Janssen, *J. Am. Chem. Soc.,* 2015,**137,** 2231 – 2234

23. S. Arzhantsev and M. Maroncelli, *Appl. Spectrosc.,* 2005,**59,** 206 - 220